Comparative Performance Evaluation of Magnetron Sputtered TiN, AlCrN, and TiAlCrN Coatings

Baitsi Paula Montwedi, Samson Olaitan Jeje, Mxolisi Brendon Shongwe

Department of Chemical, Metallurgical and Materials Engineering, Faculty of Engineering and Built Environment, Tshwane University of Technology, Pretoria 0001, South Africa.

Abstract

This study presents a comparative performance evaluation of magnetron-sputtered TiN, AlCrN, and TiAlCrN coatings on tool steel substrates. Coatings play a pivotal role in enhancing the durability of engineering components exposed to harsh conditions. TiN is known for outstanding hardness and durability, AlCrN for superior wear resistance, and TiAlCrN for exceptional thermal stability and oxidation resistance. The substrate (EN 1.2363) underwent PVD coating using a closed-field unbalanced magnetron sputter ion plating (CFUBMSIP) process in a water-cooled stainless-steel vacuum chamber with four magnetron ports, operating for 3 hours per batch followed by 12 hours of natural convection cooling, utilizing TiN, AlCrN, and TiAlCrN films deposited for 180 minutes in an Ar and nitrogen atmosphere. X-ray diffraction (XRD) revealed distinctive crystal structures, with all coatings exhibiting a common preferred orientation of the (111) plane and TiAlCrN showing a ternary nitride phase. Scanning electron microscopy (SEM) images displayed the compact nature of TiAlCrN with finer grains, while TiN exhibited a densely compacted with no evidence of delamination and AlCrN showed denseness with smaller grains. Nano-indentation test was conducted to assess the coatings' hardness and elastic modulus. TiAlCrN exhibited the highest hardness (3091±243 HV), highest elastic modulus (369.86±54.19 GPa), and the best wear rate (0.1887 x 10^{-4} mm^3/Nm^{-1}) suggesting potential suitability for applications demanding superior rigidity and wear resistance. The study provides valuable insights for materials scientists and engineers in optimizing coating selection for specific applications.

Keywords: *Magnetron Sputtering, TiAlCrN, Thin film deposition, Nanoindentation, Hardness*.

1. Introduction

Coatings are crucial in improving the performance and durability of engineering components (e.g. tool steels) that are exposed to harsh operating conditions, such as extreme temperatures, corrosive surroundings, and abrasive erosion. Titanium carbide (TiC) was one of the initial compounds utilized in coatings application due to its exceptional hardness via the chemical vapor deposition (CVD) technique [1]. However, the high temperature required for this process made it impractical for use on steel substrates, limiting its application primarily to solid carbide tools [2]. Physical vapor deposition (PVD) techniques, specifically magnetron sputtering, have become a promising method for depositing uniform and well-adhered thin films. PVD aimed to lower the processing temperature of coatings to below 550 °C, allowing for the application of coatings on high alloy steels [3]. These coatings provide a range of benefits, such as increased hardness, improved wear resistance, and enhanced corrosion resistance. This makes them extremely valuable for use in cutting tools, aerospace components, and other important engineering systems.

Common industrial methods used to enhance the mechanical properties of tool steel surfaces include

Corresponding author: *Samson Olaitan Jeje (jejesamsonn@gmail.com)*
Received: *11 March 2024*; Revised: *20 April 2024*; Accepted: *24 April 2024*; Published: *30 April 2024*

surface hardening, nitridation, surface coating, and laser surface treatment. Various studies have demonstrated the potential for enhancing the durability and effectiveness of hot work tools through the utilization of surface treatment techniques, including plasma nitriding, PVD coating, or a combination of these methods [4-10]. For over a decade, PVD TiN has been a widely utilized compound due to the ease of controlling nitriding reactions making it a popular choice for applications requiring enhanced mechanical properties [2, 11]. Titanium nitride (TiN), aluminium chromium nitride (AlCrN), and titanium aluminium chromium nitride (TiAlCrN)are coating materials that have attracted considerable interest because of their distinct properties and broad applicability across different industrial sectors.

Researchers seek PVD coatings in their pursuit of superior tools and components. This has led to several studies providing insights on how to optimize these coatings for specific applications. Bobzin et al. [10] conducted a study specifically on the cyclic impact fatigue of PVD coatings applied to tool steel substrates. They revealed that the interplay between coating thickness, morphology, residual stress, and plastic deformation determines fatigue life. Moderate compressive stress and controlled thickness in thin coatings, particularly those with higher aluminium content, can significantly delay crack initiation. This study emphasizes the significance of tailoring coating properties for fatigue-resistant tools in cyclic impact environments. Herrera-Jimenez et al. investigated the impact of the interface engineering techniques on the performance of TiN coatings on Ti-6Al-4V alloys. Ar plasma, Ti implantation, and surface nitriding were employed, each influencing the coating's microstructure, texture, and residual stress. Notably, the study identified a strong anisotropy in the residual stress depending on the substrate clamping method, highlighting a crucial factor to consider during deposition. Overall findings suggest that interface engineering can significantly enhance the mechanical properties and adhesion of TiN coatings, paving the way for improved component durability.

Feng et al. [12] explored the mechanical performance of various PVD coatings on 9Cr18 steel. Their study revealed that TiN/TiNC emerged as a promising wear-resistance candidate. This coating exhibited a remarkable combination of high adhesion force, low friction coefficient, and superior wear resistance compared to TiN alone. Hence, the coating holds potential applications in cutting tools and wear pads. All studies highlight the diverse strategies and considerations in optimizing PVD coatings for specific applications. By understanding the interplay between coating properties, interface engineering, and mechanical properties, researchers can tailor PVD coatings for enhanced performance and durability, ultimately leading to more efficient, and long-lasting tools and components.

The choice of TiN, AlCrN, and TiAlCrN coatings is based on their widespread use in industrial applications and the requirement to differentiate their nuanced performance attributes. TiAlCrN is distinguished by its exceptional thermal stability and resistance to oxidation [13, 14], while AlCrN is renowned for its superior ability to withstand wear [15, 16]. Meanwhile, TiN is a widely used benchmark coating due to its exceptional hardness and durability [17]. To ensure the study's relevance and impact, it's crucial to highlight the significance of comparing TiN, AlCrN, and TiAlCrN coatings. These coatings play a pivotal role in enhancing the durability of engineering components in harsh conditions. Surface treatment techniques like PVD coating are essential for improving mechanical properties across industries. Analyzing these coatings using magnetron sputtering provides insights into their physical and mechanical properties. Understanding these attributes enables informed coating selection and optimization for better performance in real-world applications. This study contributes to materials engineering innovation by advancing our understanding of coating performance for more efficient tools and components, and also assisting materials scientists and engineers in making well-informed decisions for specific applications. This study examines the comparative performance assessment of TiN, AlCrN, and TiAlCrN coatings fabricated using magnetron sputtering. The selected coatings encompass a range of compositions, each bestowing unique mechanical and structural characteristics to the surfaces they are applied on. The main objective of this investigation is to clarify and compare the physical and mechanical properties of these coatings using a wide range of analytical techniques.

2. Experimental Methods

2.1. Preparation of Substrate

The toolsteel (EN1.2363) with chemical composition as shown in Table 1 was used as substrate. The heat

treatment process was done under vacuum with nitrogen gas in a Schmetz (GmbH, Denmark) vacuum furnace. The first step was the hardening of the toolsteel, which was done at the austenizing temperature of 970°C. Heating the toolsteel to 970°C increases its mechanical qualities for further processing due to enhanced carbon content in the matrix and increased dissolution of primary carbides [18]. This is followed by a three-stage tempering process at 280°C, with the first stage entailing quenching at 3 bars and the rest at 2 bars. This is more aligned with the EN1.2363 heat treatment process with more pre-treatment and tempering, thereafter the toolsteel specimens are pre-cleaned and treated. The hardening was subsequently followed by the pre-cleaning of the steel substrates to ensure adequate adhesion, through steam cleaning followed by ultrasonic cleaning for 190 seconds at 49°C. This was done through a series of cleaning and rinsing stages until the last drying stage. The ultrasonic bath was made up of an alkaline-based agent, salt, and demineralized water.

Table 1. Substrate's (toolsteel) chemical composition in weight percentage (w/w%).

Element	C	Si	Mn	Cr	Mo	V
Concentration (w/w%)	1.00	0.30	0.55	5.20	1.10	0.25

2.2 PVD Coating

The substrate was coated in a vacuum chamber in the PVD coating machine supplied by Teer Coatings Limited (Droitwich, UK), utilizing CFUBMSIP. The PVD coating was achieved through magnetron sputter ion plating in a water-cooled stainless-steel vacuum chamber consisting of four magnetron ports (two of which are kept as reserves) as illustrated in Figure 1 (a). The schematic depiction of the flow mechanism of the equipment is shown in Figure 1 (b). The PVD coating machine's environmental and equipment settings are shown in Table 2. The PVD coating process takes 3 hours per batch, followed by cooling through natural convection for another 12 hours. The magnetron ports in the unbalanced magnetron sputter ion plating system are arranged such that adjacent ports are of the opposite polarity and are designed to bombard the specimens with high-intensity ions under a magnetic field during coating [19]. Before the coating process commences, the vacuum gases (Argon and nitrogen) are released, and the chamber is vented. TiN, AlCrN, and TiAlCrN films were deposited for 180 min in the Argon and nitrogen atmosphere. The coated substrates were then unloaded, and the o-ring was cleaned, but the chamber was kept under vacuum to maintain a positive pressure.

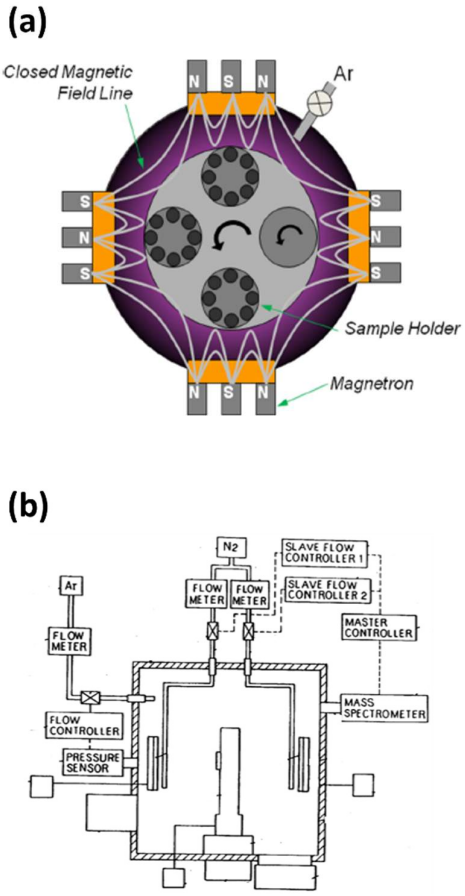

Figure 1. (a) Magnetron sputter assembly; (b) The flow mechanisms of the internal chamber.

2.3 Surface preparation and characterization

The cross-section of the coated toolsteel samples was prepared using more abrasive means of wet polishing for accurate analyses of the microstructures. This was using a Struers (USA) Tegramin-30 semi-automatic materialographic surface preparation grinder and polisher [20] to ensure that the test pieces could be polished in bulk, whilst providing a consistent surface. The samples were prepared in line with ASTM E3-01. The coating morphology was characterized utilizing scanning electron microscopy (SEM) JOEL JSM IT 100 (Japan). X-Ray diffraction (XRD) analyses were carried out on an Empyrean Model of the PANalytical X-Ray Diffractor (Malvern PANalytical, UK) using these settings: (Cu_Kα radiation at 40kV/ 45 mA, 2θ range = 5–90°, λ = 0.154 nm, count time = 1 s for 0.017° step).

Table 2. The environmental and equipment settings for the PVD coating machine.

Environment Settings		**Equipment Settings and Requirements**					
Temp. Max, working (°C)	Deposition Temp. (°C)	Magnetron Target Size (mm)	Base Vacuum (mbar)	Shaft Speed (rpm)	Process Gas 1	Process Gas 2	Bias Power (kW)
1050	400	133 x 330	3 x 10-5	1-10	Ar (99.998 %)	N2 (99.998 %)	5

2.4 Mechanical Tests

Nano-indentation was employed through Load and penetration depth techniques using a diamond tipped, Berkovich indenter which had a nominal radius of 150 nm. The method used is based on the Oliver-Pharr method, which consists of a series of loading cycles [19]. The tests were conducted on the NHT3 (Anton-Paar, GmbH) nano-indenter using the Indentation 8.0.23 software. 10 measurements were conducted for each coated sample. The output variables obtained were the Indentation hardness and Elastic Modulus determined using the force-displacement curves obtained at the maximum indentation force of 400 mN, rate of 1200 mN/min, and time of 60s.

2.5 Wear test

The wear characteristics of the newly coated samples were evaluated by subjecting them to testing using an Anton Paar TRB3 pin-on-disc Tribometer under ambient conditions. In this experimental configuration, a counter ball made of 100Cr6 steel was subjected to circular motion against the coated samples. The load applied was 20 N, with a radius of 0.03 mm and an acquisition rate of 15 Hz. No lubrication was used during the experiment.

3. Results and Discussion

3.1 XRD characterization of coatings

XRD measurements were performed to determine the crystal structure of the coatings. In Figure 2, the XRD patterns of TiN, AlCrN, and TiAlCrN synthesized by magnetron sputtering are presented. The XRD pattern TiN coating (Figure 2a) exhibits prominent peaks at around 2θ angle of 36.69° and 42.10°, which corresponds to the (111) and (200) crystallographic plane reflection respectively. This peak is accompanied by a supplementary ensemble of peaks for various TiN (220), (311), and (222) planes at 2θ angles of, 60.96°, 73.22°, and 77.76° respectively. The 2θ angles are very close to the ones obtained by Herrera-Jimenez et al. [21]. TiN films deposited using PVD processes generally exhibit growth in three specific crystallographic orientations, namely (200), (111), and (220) [22]. The XRD shows there are no (or a limited presence that is not detected) secondary phases such as TiO2. This demonstrates proficient management of the deposition process and an ample nitrogen supply throughout the creation of the film. The presence of strong and well-defined peaks, together with favorable intensity ratios, indicates a good degree of crystallinity in the TiN film [23].

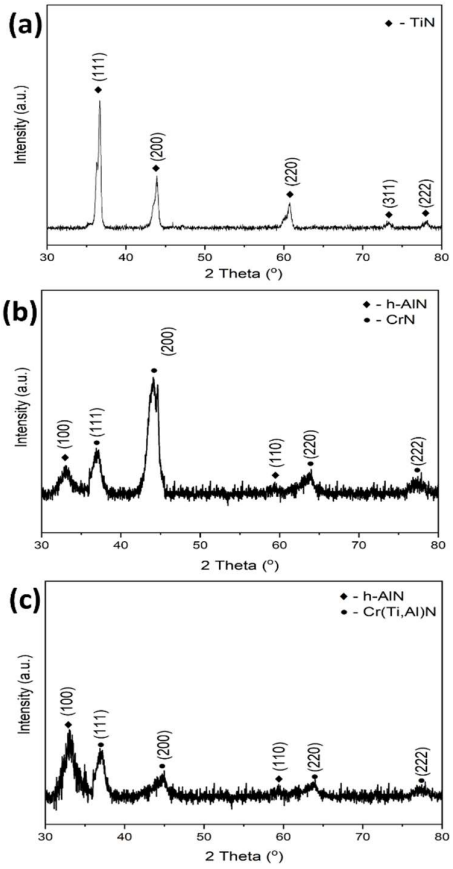

Figure 2. XRD patterns of coatings: (a); TiN (b) AlCrN and (c) TiAlCrN.

XRD pattern of the AlCrN coating showed that two major crystal structures namely B1 NaCl cubic structure CrN-based (CrN) with diffraction planes (111), (200), (220), and (222); and hexagonal close-packed structure AlN-based (h-AlN) with diffraction planes (100) and (110) are detected in the coatings. The observed CrN-based diffraction plane (200) has the highest intensity. Compared to the TiN pattern, the AlCrN pattern also exhibits a strong peak at 2θ angles of 44.08°, suggesting (200) plane as the preferred orientation. This indicates a common texture development despite the different coating materials. In addition, the AlCrN pattern has a wider and less prominent peak at the (111) diffraction plane which can be attributed to the presence of secondary phases of Al or Cr oxides [15], which might have been generated as a result of residual oxygen in the deposition chamber. The broader main peak observed in AlCrN also suggests potentially lower crystallinity in the AlCrN film compared to the TiN film [23].

The TiAlCrN pattern has a strong peak around 38° 2θ angle, just like the TiN and AlCrN patterns. This suggests that the (111) plane is the preferred orientation. This shows a similar texture development, even though the coatings are different. The prominent peaks are found at 2θ angles of 33.03° and 36.89°, which corresponds to the (100) and (111). Similar to the AlCrN pattern, the main peak in the TiAlCrN pattern appears broader than the TiN peak. This also suggests potentially lower crystallinity in the TiAlCrN film compared to the TiN film [23]. The strong (111) preferred orientation for all three coatings (TiN, AlCrN, and TiAlCrN) suggests that the CFUBMSIP deposition process might favor this texture development for various materials.

3.2 SEM characterization of coatings

The plain view and cross-section of all the coatings are shown in Figure 3. The surface of the TiN coating (Figure 3a) shows a densely compacted structure with the distribution of defects in the form of pin holes. These could be small secondary phase inclusions or surface contaminants. The dense and continuous film with well-defined grains suggests good adhesion, crystallinity, and potentially good mechanical properties like hardness and wear resistance properties [19]. The AlCrN coating (Figure 3b) appears relatively dense and continuous with the grain size appearing smaller compared to TiN coating. This can be attributed to the presence of Al and Cr that brought about growth inhibition. The AlCrN suggests good crystallinity but there are some areas with smaller grains or even voids, suggesting slightly less uniformity compared to the TiN coating. There are a few isolated brighter spots and darker regions scattered throughout the image. These could be small secondary phase inclusions or surface contaminants, potentially including oxides of Al or Cr.

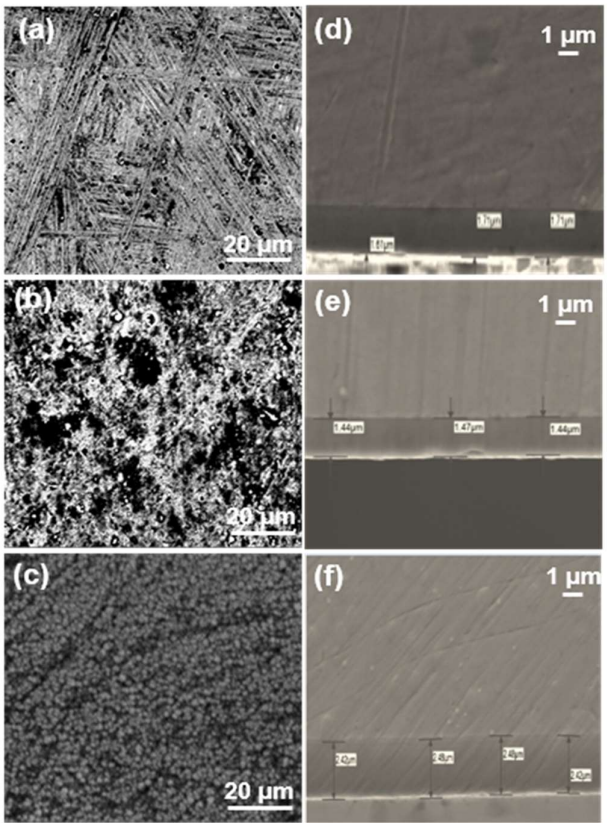

Figure 3. SEM images of TiN, AlCrN, and TiAlCrN coatings: plain-view (a, b, and c respectively) and cross-section (d, e, and f respectively).

In the case of the TiAlCrN-coating morphology in Figure 3c, the coating appears compact and made of smaller grains. the SEM images do not show the typical macro-particles typical of coating processes such as cathodic arc evaporation as observed in the study of Varghese et al. [16] and Kong et al. [24]. These defects would be detrimental in a high-speed steel and high-volume striking environment, as these particles would dislodge and become imprinted as a defect into the design of the embossed product. The surface texture of the film is generally smooth, with even fewer prominent

protrusions or defects compared to the other coatings. This suggests a potentially smooth interface with the substrate. The microstructure of the composite structures of the coated substrates is shown cross-sectionally in Figures 4d, 4e, and 4f for TiN, AlCrN, and TiAlCrN respectively. The coated layer thickness ranges on the cross-sectioned specimen: 1.61 – 1.71 µm for TiN, 2.57 – 2.63 µm for AlCrN, and 2.42 – 2.48 µm for TiAlCrN coating.

The combined effect of the heat treatment/high hardening temperature (970°C hardening followed by 280°C tempering), pre-cleaning (Steam and ultrasonic cleaning with an alkaline agent), and PVD coating process (CFUBMSIP) is responsible for having a well-adhered, well-crystallized coating on the tool steel substrate with potentially good mechanical properties. This aligns with the XRD and SEM analysis.

3.3 Mechanical properties of coatings

Depth penetration was done based on the Oliver-Pharr method, which is derived from the tangent line to the upper portion of the unloading curve [19] and is therefore expressed through a power relation, as:

$$P = A(h - h_f)^m \quad (1)$$

Where, P is the maximum load (mN), and h_f is the residual depth or maximum displacement between the loading and unloading curves, h is the elastic displacement, with A and m being the empirical constants of the tangent line. Unloading curves obtained from the Load versus penetration depth curves are therefore mostly derived using the Oliver-Pharr method. Other relations are adapted to minimize the effects of thermal drift and plastic reversion [19]. In this study, all unloading curves 'mimicked' the Oliver-Pharr derivation. Depth penetration curves obtained from nano-indentation tests conducted on the surfaces of the coated substrates, using the Anton Paar (NHT3) are shown in Figure 4.

The depth of the impact in the nano-indentation test was less than 1163 nm, which is about half of the thickness of the coatings. In this case, it means that the given hardness is a combination of the base and composite layers [25]. The maximum penetration depths of the coatings are 960.63 nm, 1102.32 nm, and 1162.12 nm for TiAlCrN, AlCrN, and TiN respectively. The observed differences in penetration depth between TiN, AlCrN, and TiAlCrN coatings likely stem from a combination of factors related to material properties and microstructure.

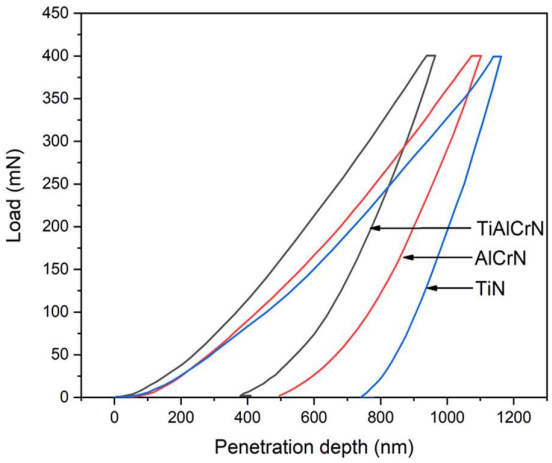

Figure 4. Load-unload curves of TiN, AlCrN, and TiAlCrN coatings.

In general, an increase in hardness results in a decrease in penetration depth when subjected to the same load, and this is known as the indentation size effect (ISE) [26]. By comparing the existing hardness values: TiN has ~15-35 Gpa [27-30], AlCrN has ~20-40 Gpa [31, 32], and TiAlCrN has ~25-45 GPa [33, 34]. Similarly, a higher Young's modulus indicates greater stiffness and resistance to elastic deformation [35, 36], leading to lower Penetration depth. Based on these ranges, the lowest penetration depth of TiAlCrN coating can be attributed to the highest combined hardness and modulus. Also, Finer grain sizes and lower defect densities generally enhance mechanical properties like hardness and modulus. The SEM images (Figure 3) reveal that TiAlCrN exhibits finer grains compared to TiN and AlCrN.

Figure 5 shows the nanoindentation hardness (HV0.005) and elastic modulus (GPa) of all the coating. The hardness of the coating is dependent on its structure. The indentation hardness of TiN, AlCrN, and TiAlCrN are 1991±211, 2371±250, and 3091±243 HV respectively. The trend in hardness and penetration depth aligned confirming the earlier values from several studies. That is, higher hardness leads to greater resistance to indentation, resulting in lower penetration depth. This explains why TiAlCrN with the higher hardness has the lowest penetration depth, and TiN with the lower hardness has the highest penetration depth. TiN exhibits a Cubic NaCl

structure as depicted in Figure 6a with Ti and N atoms occupying alternating lattice sites. This simple structure offers a decent hardness. AlCrN exhibits a cubic NaCl structure similar to TiN, but with Al and Cr substituting for some of the Ti atoms. Hence, the introduction of hexagonal AlN (h-AlN) and CrN phase as seen in the XRD analysis (Figure 2b), and the possibility of a minor Cr2N phase (not detected from XRD result). This could introduce lattice distortion and solid solution strengthening, thus enhancing the hardness [37, 38]. Based on the XRD analysis (Figure 2c), TiAlCrN exhibited a ternary nitride phase where Cr replaces some of the Ti or Al sites in a TiAlN lattice as depicted in Figure 6b. There is the possibility of the transformation of the cubic NaCl structure to a refined and defect-free Wurtzite structure of Ti-(Al, Cr)N phase where Ti shares its lattices with both Al and Cr. This phase exhibits a higher hardness than the cubic structure due to its intrinsic crystal structure and additional strengthening mechanisms like twinning [39, 40].

The elastic modulus of the coatings is also found to follow the same trend as the hardness. Similarly, the presence of Al and Cr in AlCrN and TiAlCrN contributes to stronger bonds and potentially denser packing compared to TiN. Additionally, the wurtzite phase in TiAlCrN might further enhance its stiffness due to its inherent crystal structure. The higher elastic modulus of TiAlCrN suggests it might be more suitable for applications requiring high rigidity and minimal elastic deformation, such as cutting tools and other wear-resistant coatings.

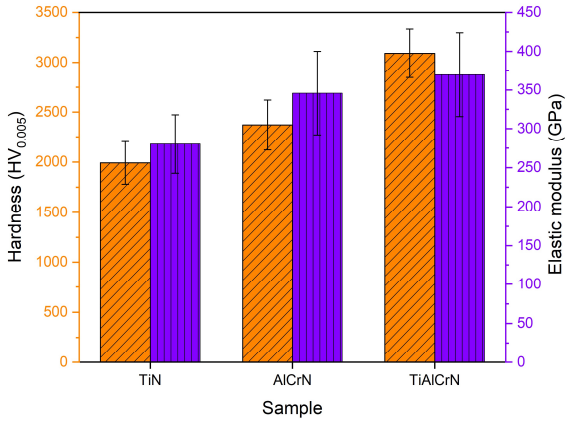

Figure 5. Nanoindentation hardness and elastic modulus of TiN, AlCrN, and TiAlCrN coatings.

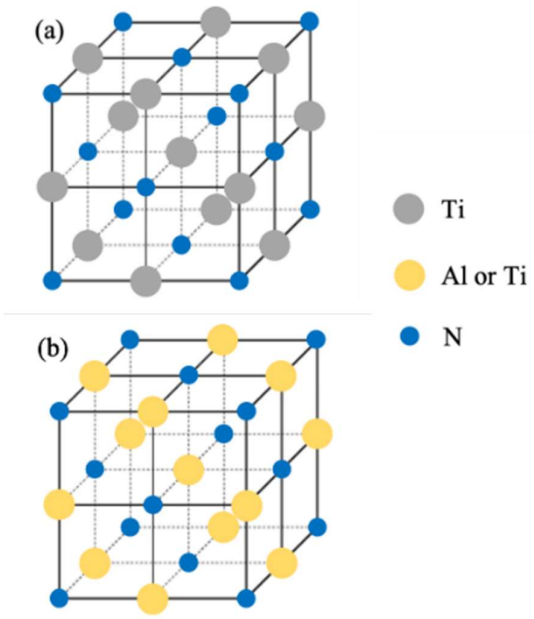

Figure 6. The Cubic NaCl structure representation of: (a) TiN and; (b) TiAlN [41].

3.4. Wear properties of coatings

Figure 7a illustrates the friction coefficients (COF) with sliding time, while Figure 7b shows the average COF acquired from the tribometer for each of the coated work parts for one hour. The tests were conducted at a speed of 100 rpm and a force of 20N. This was done since the lifespan of the tooling was a variable of interest, and the longevity of tooling in high-speed steel's mechanical processes is crucial. Overall, in the early stages, the COF experiences a rapid rise until it reaches its maximum value, followed by a transition to a stable value. The initial high coefficient of friction may be attributed to the adhesive transfer of material from the coating to the counterface or vice versa and the surface roughness [15]. This transfer can result in increased friction as the surfaces come into contact and interact. TiAlCrN coating has the COF peaked at 0.37, followed by a gradual decrease before it stabilizes at around 0.30 (sliding time of 700 s). This frictional force stabilizes once a significant portion of the test area is covered with the transferred material [42]. The stabilization of the COF value of AlCrN started at the early stage, however, the was a sudden 'jump' around 265 s sliding time from COF of 0.25 to 0.46 where it finally stabilizes. This spike can be caused by surface irregularities. Stefan et al. [43] suggested the formation of debris might be responsible. TiN coating displayed a

relatively higher and more fluctuating COF until it stabilizes around 0.56. This suggests that the TiN coating experienced higher frictional resistance and fluctuations in the interaction between the coated sample and the counter ball.

TiAlCrN coated sample exhibited the lowest average COF (0.3014), indicating smoother sliding behavior compared to TiN (0.514) and AlCrN (0.456). This lower COF suggests reduced frictional resistance and potentially lower energy losses during sliding contact, which is advantageous for applications where energy efficiency is critical. The values of the COFs for AlCrN and TiN coatings obtained in this work are related to that of heat-treated AlCrN coatings by Cadena et al. [44] and TiN coatings by Baldin et al [45]. The low and stable COF values suggest that the TiAlCrN-coated sample possesses the best wear resistance in comparison to other samples.

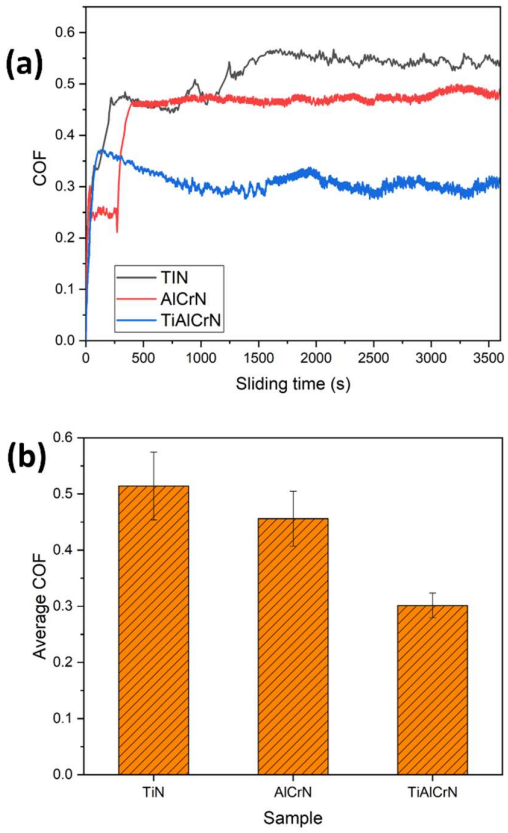

Figure 7. The plot of: (a) COF vs sliding time of samples; (b) Average COF of samples.

Figure 8 depicts the wear rate of all coated samples. As expected from the COF results, TiAlCrN demonstrated the lowest wear rate (0.1887 x 10^{-4} mm^3/Nm^{-1}), signifying superior wear resistance compared to TiN (0.6365 x 10^{-4} mm^3/Nm^{-1}) and AlCrN (0.3543 x 10^{-4} mm^3/Nm^{-1}). The enhanced wear resistance of TiAlCrN can be attributed to its exceptional thermal stability and oxidation resistance [13], which may inhibit material loss and surface degradation under sliding contact conditions. In addition, the outstanding wear resistance of TiAlCrN can also be attributed to its composition, including the combination of TiN, AlCrN, and TiCN, which results in high hardness, low friction, and strong metallic bonding. These factors collectively contribute to the superior wear performance of TiAlCrN compared to other coatings like TiN and AlCrN.

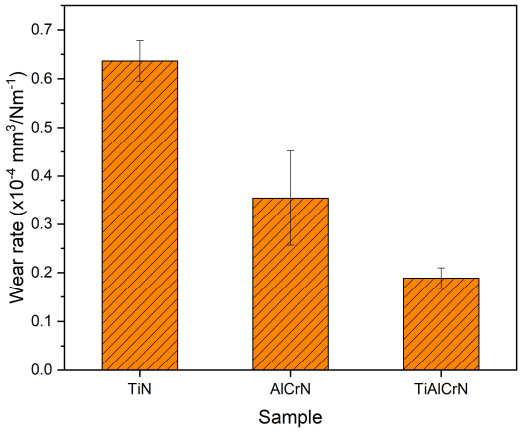

Figure 8. The wear rate of the coated samples.

4. Conclusion

In this comparative assessment, TiN, AlCrN, and TiAlCrN coatings were successfully fabricated through magnetron sputtering. The key conclusions drawn are stated below:

- The coatings' crystal structures were examined using X-ray diffraction (XRD), revealing a commonly preferred orientation of the (111) plane for all coatings. TiAlCrN exhibited a ternary nitride phase, suggesting unique structural characteristics.
- Scanning electron microscopy (SEM) images showcased distinct surface morphologies. TiAlCrN displayed a compact structure with finer grains, while TiN exhibited a densely packed pattern with the distribution of defects in the form of pinholes, and AlCrN showed denseness with smaller grains.

- Nano-indentation tests for hardness and elastic modulus revealed that TiAlCrN exhibited the highest hardness (3091±243 HV) and elastic modulus among the coatings, making it a promising candidate for applications requiring superior rigidity and wear resistance.
- TiAlCrN exhibited the lowest wear rate among the coatings, indicating superior wear resistance compared to TiN and AlCrN. The exceptional thermal stability and oxidation resistance of TiAlCrN might have contributed to its enhanced wear resistance.

The study concluded that while the TiAlCrN coating exhibited exceptional hardness, potential crystal structure transformations, and resistance to indentation, it's important to note that the performance of TiN and AlCrN coatings was also notable. The comparative analysis offered valuable insights for materials scientists and engineers in tailoring coating selection for specific applications based on their nuanced performance attributes.

Acknowledgments

The authors acknowledge the research facilities support in part for this research by the Faculty of Engineering and Built Environment, Tshwane University of Technology, and the Department of Chemical, Metallurgical, and Materials Engineering of the Tshwane University of Technology, Pretoria, South Africa.

Competing Interest Statement

The authors declare that they have no known competing financial interests or personal relationships that could have influenced the work reported in this paper.

Data Availability Statement

The datasets used and/or analyzed during the current study are available from the corresponding author on reasonable request**.**

References

[1] T. Takahashi, K. Sugiyama, and K. Tomita, "The chemical vapor deposition of titanium carbide coatings on iron," *Journal of the Electrochemical Society,* vol. 114, no. 12, p. 1230, 1967.

[2] R. A. Mesquita and C. A. Schuh, "Tool steel coatings based on niobium carbide and carbonitride compounds," *Surface and Coatings Technology,* vol. 207, pp. 472-479, 2012.

[3] W. Schintlmeister, W. Wallgram, and J. Kanz, "Properties, applications and manufacture of wear-resistant hard material coatings for tools," *Thin Solid Films,* vol. 107, no. 2, pp. 117-127, 1983.

[4] S.-H. Chang, K.-T. Huang, and Y.-H. Wang, "Effects of thermal erosion and wear resistance on AISI H13 tool steel by various surface treatments," *Materials Transactions,* vol. 53, no. 4, pp. 745-751, 2012.

[5] E. Bitay, L. Tóth, T. A. Kovács, Z. Nyikes, and A. L. Gergely, "Experimental study on the influence of TiN/AlTiN PVD layer on the surface characteristics of hot work tool steel," *Applied Sciences,* vol. 11, no. 19, p. 9309, 2021.

[6] P. Panjan, A. Drnovšek, P. Terek, A. Miletić, M. Čekada, and M. Panjan, "Comparative study of tribological behavior of TiN hard coatings deposited by various PVD deposition techniques," *Coatings,* vol. 12, no. 3, p. 294, 2022.

[7] K. Lukaszkowicz, A. Czyżniewski, W. Kwaśny, and M. Pancielejko, "Structure and mechanical properties of PVD coatings deposited onto the X40CrMoV5-1 hot work tool steel substrate," *Vacuum,* vol. 86, no. 8, pp. 1186-1194, 2012.

[8] Đ. Goršćak, P. Panjan, M. Čekada, and L. Ćurković, "Comparison of mechanical properties of various PVD hard coatings for forming tools," *Surface engineering,* vol. 23, no. 3, pp. 177-182, 2007.

[9] Y.-Y. Chang and S. Amrutwar, "Effect of plasma nitriding pretreatment on the mechanical properties of AlCrSiN-coated tool steels," *Materials,* vol. 12, no. 5, p. 795, 2019.

[10] K. Bobzin, C. Kalscheuer, and M. Tayyab, "Effect of CrAlN coating properties on impact fatigue of tool steel," *Surface and Coatings Technology,* vol. 471, p. 129869, 2023.

[11] A. Baptista, F. Silva, J. Porteiro, J. Míguez, and G. Pinto, "Sputtering physical vapour deposition (PVD) coatings: A critical review on process improvement and market trend demands," *Coatings,* vol. 8, no. 11, p. 402, 2018.

[12] X. Feng, Y. Zhang, H. Hu, Y. Zheng, K. Zhang, and H. Zhou, "Comparison of mechanical behavior of TiN, TiNC, CrN/TiNC, TiN/TiNC films on 9Cr18 steel by PVD," *Applied surface science,* vol. 422, pp. 266-272, 2017.

[13] Y. X. Xu, H. Riedl, D. Holec, L. Chen, Y. Du, and P. H. Mayrhofer, "Thermal stability and oxidation resistance of sputtered TiAlCrN hard coatings," *Surface and Coatings Technology,* vol. 324, pp. 48-56, 2017.

[14] S. Zuo *et al.*, "Effect of plasma carbonitriding on the high-temperature tribological properties of a TiAlCrN coating

on 300M steel by multi-arc ion plating," *Philosophical Magazine,* vol. 101, no. 10, pp. 1188-1201, 2021.

[15] F. Ahmad, L. Zhang, J. Zheng, I. Sidra, and S. Zhang, "Characterization of AlCrN and AlCrON coatings deposited on plasma nitrided AISI H13 steels using ion-source-enhanced arc ion plating," *Coatings,* vol. 10, no. 4, p. 306, 2020.

[16] V. Varghese, K. Akhil, M. R. Ramesh, and D. Chakradhar, "Investigation on the performance of AlCrN and AlTiN coated cemented carbide inserts during end milling of maraging steel under dry, wet and cryogenic environments," *Journal of Manufacturing Processes,* vol. 43, pp. 136-144, 2019.

[17] M. to Baben, M. Hans, D. Primetzhofer, S. Evertz, H. Ruess, and J. M. Schneider, "Unprecedented thermal stability of inherently metastable titanium aluminum nitride by point defect engineering," *Materials Research Letters,* vol. 5, no. 3, pp. 158-169, 2017.

[18] H. K. Moon, K. B. Lee, and H. Kwon, "Influences of Co addition and austenitizing temperature on secondary hardening and impact fracture behavior in P/M high speed steels of W–Mo–Cr–V (–Co) system," *Materials Science and Engineering: A,* vol. 474, no. 1-2, pp. 328-334, 2008.

[19] J. Yang, M. Odén, M. Johansson-Jõesaar, and L. Llanes, "Grinding effects on surface integrity and mechanical strength of WC-Co cemented carbides," *Procedia CIRP,* vol. 13, pp. 257-263, 2014.

[20] Struers, "Tegramin-25/-30 Instruction Manual," S. Denmark, Ed., ed, 2018.

[21] E. J. Herrera-Jimenez, E. Bousser, T. Schmitt, J. E. Klemberg-Sapieha, and L. Martinu, "Effect of plasma interface treatment on the microstructure, residual stress profile, and mechanical properties of PVD TiN coatings on Ti-6Al-4V substrates," *Surface and Coatings Technology,* vol. 413, p. 127058, 2021.

[22] K. Khojier, H. Savaloni, E. Shokrai, Z. Dehghani, and N. Z. Dehnavi, "Influence of argon gas flow on mechanical and electrical properties of sputtered titanium nitride thin films," *Journal of Theoretical and Applied Physics,* vol. 7, pp. 1-6, 2013.

[23] G. F. Harrington and J. Santiso, "Back-to-Basics tutorial: X-ray diffraction of thin films," *Journal of Electroceramics,* vol. 47, no. 4, pp. 141-163, 2021.

[24] Y. Kong, X. Tian, C. Gong, D. A. Golosov, M. Li, and Q. Tian, "Enhanced discharge and surface properties of (Ti, AlCr) N coatings by cleaning cathodic-arc chamber," *Surface and Coatings Technology,* vol. 366, pp. 41-53, 2019.

[25] J. Wu *et al.*, "Effects of magnetic field strength and deposition pressure on the properties of TiN films produced by high power pulsed magnetron sputtering (HPPMS)," *Surface and Coatings Technology,* vol. 315, pp. 258-267, 2017.

[26] S. Kucharski and S. Woźniacka, "Size effect in single crystal copper examined with spherical indenters," *Metallurgical and Materials Transactions A,* vol. 50, pp. 2139-2154, 2019.

[27] S. J. Bull, "Microstructure and indentation response of TiN coatings: The effect of measurement method," *Thin Solid Films,* vol. 688, p. 137452, 2019.

[28] L. C. Hernández, L. Ponce, A. Fundora, E. López, and E. Pérez, "Nanohardness and residual stress in TiN coatings," *Materials,* vol. 4, no. 5, pp. 929-940, 2011.

[29] R. Hahn, M. Bartosik, R. Soler, C. Kirchlechner, G. Dehm, and P. H. Mayrhofer, "Superlattice effect for enhanced fracture toughness of hard coatings," *Scripta Materialia,* vol. 124, pp. 67-70, 2016.

[30] Y. Gogotsi, *Nanomaterials handbook*. CRC press, 2006.

[31] A. Gilewicz, R. Jedrzejewski, P. Myslinski, and B. Warcholinski, "Structure, morphology, and mechanical properties of AlCrN coatings deposited by cathodic arc evaporation," *Journal of Materials Engineering and Performance,* vol. 28, pp. 1522-1531, 2019.

[32] R. Wuhrer and W. Y. Yeung, "A comparative study of magnetron co-sputtered nanocrystalline titanium aluminium and chromium aluminium nitride coatings," *Scripta Materialia,* vol. 50, no. 12, pp. 1461-1466, 2004.

[33] B. D. Beake, L. Isern, J. L. Endrino, and G. S. J. W. Fox-Rabinovich, "Micro-impact testing of AlTiN and TiAlCrN coatings," vol. 418, pp. 102-110, 2019.

[34] V. Novikov, N. Stepanov, S. Zherebtsov, and G. J. M. Salishchev, "Structure and Properties of High-Entropy Nitride Coatings," vol. 12, no. 5, p. 847, 2022.

[35] H. Czichos, T. Saito, and L. Smith, "Springer handbook of materials measurement methods," 2006.

[36] D. R. H. Jones and M. F. Ashby, "Chapter 3 - Elastic Moduli," in *Engineering Materials 1 (Fifth Edition)*, D. R. H. Jones and M. F. Ashby, Eds.: Butterworth-Heinemann, 2019, pp. 31-47.

[37] A. Roy, P. Sreeramagiri, T. Babuska, B. Krick, P. K. Ray, and G. Balasubramanian, "Lattice distortion as an estimator of solid solution strengthening in high-entropy alloys," *Materials Characterization,* vol. 172, p. 110877, 2021/02/01/ 2021.

[38] C. Lee *et al.*, "Lattice-distortion-enhanced yield strength in a refractory high-entropy alloy," vol. 32, no. 49, p. 2004029, 2020.

[39] W. D. Callister Jr and D. G. Rethwisch, *Fundamentals of materials science and engineering: an integrated approach*. John Wiley & Sons, 2020.

[40] P. V. Gaikwad and J. Bang, "Hardness and Mechanical Properties of Wurtzite B–C–N Compounds," *The Journal of Physical Chemistry C,* vol. 127, no. 5, pp. 2581-2588, 2023/02/09 2023.

[41] R. QIU, "Electron Microscopy Investigation of Detailed Microstructures of CVD TiAlN and TiN Coatings," 2020.

[42] O. P. Terleeva, A. I. Slonova, A. B. Rogov, A. Matthews, and A. Yerokhin, "Wear resistant coatings with a high friction coefficient produced by plasma electrolytic oxidation of Al alloys in electrolytes with basalt mineral

powder additions," *Materials,* vol. 12, no. 17, p. 2738, 2019.

[43] S. Valkov *et al.*, "Influence of electron beam treatment of Co–Cr alloy on the growing mechanism, surface topography, and mechanical properties of deposited TiN/TiO2 coatings," *Coatings,* vol. 9, no. 8, p. 513, 2019.

[44] N. L. Cadena, R. Cue-Sampedro, H. R. Siller, A. M. Arizmendi-Morquecho, C. I. Rivera-Solorio, and S. Di-Nardo, "Study of PVD AlCrN coating for reducing carbide cutting tool deterioration in the machining of titanium alloys," *Materials,* vol. 6, no. 6, pp. 2143-2154, 2013.

[45] V. Baldin, L. R. R. da Silva, C. R. B. Baldin, C. Augusto Neitzke, R. Diego Torres, and A. Rocha Machado, "Characterization and Performance of TiAlN and TiN Coatings on Plasma-Nitrided AISI 4140 Steel," *Materials Performance and Characterization,* vol. 10, no. 1, pp. 503-514, 2021.